Electrochemical Determination of Maleic Anhydride Using Gold Nanoparticles and Cysteine

Teh Ubaidah Noh[1], Azila Abd. Aziz[2], Nur Ayshah Rosli[3] and Nurul Izzah Khalid[4]*

[1]Institute of Bioproduct Development, Universiti Teknologi Malaysia, 81310, Skudai, Johor, Malaysia
[2]Department of Chemical and Environmental Engineering, Malaysia–Japan International Institute of Technology, Universiti Teknologi Malaysia Kuala Lumpur, Jalan Sultan Yahya Petra, 54100 Kuala Lumpur, Malaysia
[3]School of Chemical Engineering, Universiti Sains Malaysia, Engineering Campus, 14300 Nibong Tebal, Pulau Pinang
[4]Department of Food Technology, Faculty of Food Science and Technology, Universiti Putra Malaysia, 43400 Serdang, Selangor, Malaysia
*Corresponding author (e–mail: nurulizzah@upm.my)

This study introduces an innovative approach for the rapid detection of maleic anhydride haptenation in skin sensitization studies. The method involved the modification of a screen–printed carbon electrode (SPCE) with cysteine and gold nanoparticles (AuNPs) using electrodeposition and self–assembled monolayer (SAM) techniques. These modifications created an efficient platform for detecting maleic anhydride interactions. To characterize the modified SPCE, various analytical techniques were employed. The electrochemical properties of the modified SPCE were thoroughly investigated using electrochemical impedance spectroscopy (EIS) and cyclic voltammetry (CV). These techniques provided valuable insights into the detection capabilities of the modified SPCE. Notably, the (electrodeposition of AuNPs, self–assembled of AuNPs and cysteine on SPCE) ETSC modified SPCE exhibited optimal maleic anhydride detection through impedance measurements. The modified electrode demonstrated good stability at room temperature and good reproducibility, underscoring its potential as a rapid detection sensor for initial skin sensitizer screening in skincare products.

Keywords: Cysteine; maleic anhydride; screen printed carbon electrode; impedance; gold nanoparticles.

Received: January 2024; Accepted: April 2024

Maleic anhydride is a chemical compound that can trigger skin sensitization, an allergic reaction that arises when the immune system responds unusually to a substance after repeated or prolonged exposure. Upon subsequent encounters with maleic anhydride, sensitized individuals may experience a range of adverse skin reactions, including redness, itching, swelling, and, in more severe cases, the emergence of symptoms resembling dermatitis or eczema [1]. Following the Cosmetic Directives of the European Economic Community, a crucial aspect of safety evaluation for cosmetic and skincare product ingredients involves conducting a skin sensitization test [2]. Skin sensitization is characterized as an allergic response triggered by substances referred to as skin sensitizers upon contact with the skin [3]. The initial pivotal event in skin sensitization entails the covalent binding of haptens (maleic anhydride) to amino acids within nucleophiles. These haptens, which are electrophilic, low molecular weight substances reactive in nature, or metabolites, form covalent connections with nucleophilic centres (skin proteins) in peptides and are recognized by the immune system [4]. Haptenation occurs when skin proteins (cysteine, lysine, and histidine) covalently interact with haptens [5].

By modifying the screen–printed carbon electrode (SPCE) with cysteine and gold nanoparticles (AuNPs), this sensor provides a rapid and accurate means of identifying maleic anhydride. Besides the SAM method, another effective surface modification approach for the SPCE involves the electrodeposition of AuNPs. This straightforward process entails reducing a gold solution through an electrical current, forming an AuNP coating on the SPCE's surface [1,5]. Common methods for AuNP electrodeposition include impedance, voltammetry, and chronoamperometry. This study employed chronoamperometry to deposit AuNPs onto the modified SPCE carbon surface electrochemically [6]. The controlled and gradual growth of AuNPs on the electrode surface was achieved by applying a specific current. AuNPs have demonstrated their value in nanotechnology–based sensor development [3]. The combination of SAM and AuNP electrodeposition was harnessed in this study to create a highly repeatable modified SPCE for the detection of skin sensitizers, specifically maleic anhydride [1, 5].

AuNP–based SPCEs have gained popularity for their high sensitivity and selectivity in investigating electron transport mechanisms [7]. These analytical

techniques have found widespread use in recent times for gold screen printed electrodes [8], SPCEs [1, 5, 9], or hybrid carbon–gold setups [10]. The rapidity, simplicity, affordability, and accuracy inherent in electrochemical sensing make them an appealing choice for researchers [11]. Cysteine exhibits enhanced reactivity in tandem with a direct binding test for identifying skin sensitizers [1]. In this study, immobilizing cysteine on the modified SPCE working surface first involved attaching AuNPs to the surface, then creating a cysteine SAM on the AuNP layer. Cysteine is a thiol–containing amino acid, which readily binds to AuNPs, facilitating the investigation of interactions between cysteine, maleic anhydride, and AuNPs on the modified SPCE using impedance spectroscopy and voltammetry.

This study involved a comparative analysis between electrochemical impedance spectroscopy (EIS) and cyclic voltammetry (CV), with the aim of further investigating the findings previously established by Noh and Abd Aziz [1, 5]. The primary focus was on different configurations of the modified SPCEs, incorporating AuNPs and cysteine. These electrode modifications were subsequently exposed to maleic anhydride, an extreme/high skin sensitizer. The study encompassed the determination of key parameters such as fractional surface coverage (θ_{IS}^{p}), active site radius (r_a), and the distance between two adjacent sites ($2r_b$) within the context of various modified SPCE/maleic anhydride setups. CV and EIS are two distinct electrochemical techniques that offer valuable insights into different aspects of electrochemical systems [12]. CV is particularly advantageous for studying rapid electron transfer kinetics and redox reactions, providing qualitative information about reversibility and reaction mechanisms through its visual voltammograms. Its simplicity and quick data acquisition make it suitable for swift analyses and initial screening. However, CV's limited frequency–dependent information restricts its ability to analyze complex interfaces and diffusion processes comprehensively [7]. On the other hand, EIS excels in characterizing intricate electrode interfaces, offering detailed quantitative data about charge transfer resistance, double–layer capacitance, and diffusion phenomena. With its broad frequency range, EIS provides insights into various timescales of electrode processes [13]. While EIS demands a more sophisticated experimental setup and data interpretation, it offers a non–destructive means to study long–term stability and the impacts of surface modifications [14]. The choice between CV and EIS hinges on the research objectives and the specific electrochemical system. CV is suitable for researchers interested in understanding fast kinetics and gaining qualitative insights [15]. Conversely, EIS takes precedence when an in–depth analysis of interface properties, charge transfer resistance, and diffusion processes is crucial.

The comparative analysis between electrochemical impedance spectroscopy (EIS) and cyclic voltammetry (CV) offered deeper insights into the interactions between the modified SPCE, maleic anhydride, and skin proteins. This investigation enhanced our understanding of the underlying electrochemical processes and helped determine the optimal configuration for detecting skin sensitizers. EIS offered advantages over surface plasmon resonance, including heightened sensitivity, cost–effectiveness, label–free analysis, and simplicity [11]. Additionally, in this work, field emission scanning electron microscopy (FESEM), Fourier Transform infrared spectroscopy with attenuated total reflectance (FTIR–ATR), and atomic force microscopy (AFM) were employed to explore the surface morphology of the ETSC modified SPCE containing maleic anhydride. The effects of maleic concentration, stability, and reproducibility of the ETSC modified SPCE were also assessed. The SPCE was modified with layers of AuNPs, thiourea, and cysteine to determine the most suitable modified SPCE capable of detecting maleic anhydride. The successful integration of various techniques and approaches underscores the sensor's potential to revolutionize the field of skin sensitization testing, contributing to safer cosmetic and skincare product development while reducing dependence on animal testing [16].

MATERIALS AND METHODS

Chemicals and Materials

Gold (III) chloride solution ($HAuCl_4$), potassium chloride (KCl), potassium ferricyanide ($K_3Fe(CN)_6$), trisodium citrate dehydrate ($Na_3C_6H_5O_7$), cysteine ($C_3H_7NO_2S$), and maleic anhydride ($C_4H_2O_3$) were obtained from Sigma–Aldrich, Malaysia. The apparatus used in this study consisted of a SPCE with carbon as the working and auxiliary electrodes, and a silver/silver chloride reference electrode, obtained from Metrohm Malaysia [1, 5].

Preparation of the Modified SPCE

The unmodified SPCE was cleaned using an 85 % ethanol solution to eliminate any residual dirt from the surface. Subsequently, the SPCE underwent a thorough washing process and was allowed to dry in a petri dish under a controlled airflow for several minutes before being used in the experiments.

Electrodeposition of AuNPs and Cysteine on SPCE (assigned as EC Modified SPCE)

The first layer of the modified SPCE was formed through the electrodeposition of 100 µL of AuNPs and $Na_3C_6H_5O_7$ solutions (to reduce AuNPs size) using chronoamperometry with a current of +1.1 V applied

for 60 s, controlled by the GPES software. The AuNPs and $Na_3C_6H_5O_7$ solutions were prepared by heating 300 mL of 0.5 mM $HAuCl_4$ and adding 30 mL of 38.8 mM $Na_3C_6H_5O_7$ solution. Initially, the mixture appeared colourless but gradually darkened over approximately 10 minutes with further heating. The solution was then removed from the heat source and allowed to cool until a deep red colour appeared, indicating formation of the AuNP solution. Subsequently, 6 µL of 50 mM cysteine was placed over the modified SPCE and dried in a petri dish under controlled airflow to minimize oxygen exposure [1, 5, 9] (see Figure 1 (a)).

Electrodeposition of AuNPs, Self–assembly of AuNPs and Cysteine on SPCE (assigned as ETSC Modified SPCE)

The electrodeposition process for the AuNP layer on the modified SPCE was constructed similar to the 2.2.1 fabrication method (see Figure 1 (b)). Then, the modified SPCE was deposited with 6 µL of 0.25 mM thiourea as a crosslinker between the AuNP monolayers and dried under airflow. Next, the third layer was self–assembled AuNP modified SPCE. 6µL of 0.1 M cysteine, 0.001 M $HAuCl_4$, and 0.5 M H_2SO_4 were dropped on the surface of the modified SPCE in a petri dish and left to dry. Lastly, 6 µL of 50 mM cysteine was placed on the modified SPCE and allowed to dry for 30 minutes [1, 5, 9].

Electrodeposition of AuNPs, Double Self–Assembly of AuNPs and Cysteine on SPCE (assigned as ETSTSC Modified SPCE)

A similar procedure to that of the ETSC modified SPCE was conducted up to the self–assembled AuNP layer. Subsequently, the deposition of thiourea on the modified SPCE was repeated, followed by the self–assembly of AuNPs on the modified SPCE using the same quantity of chemicals. Finally, a 50 mM cysteine solution (6 µL) was dropped onto the modified SPCE [1, 5, 9] (see Figure 1 (c)).

Electrochemical Measurements

Cyclic voltammetry (CV) and electrochemical impedance spectroscopy (EIS) serve as valuable tools for evaluating the interaction of the modified SPCE/ maleic anhydride, as interpreted through the analysis of ΔR_{CT} data. The experimental frequency range spanned from 15,000 Hz to 0.01 MHz, employing +1.0 V potential and 5 mV amplitude. This analysis was conducted using an Autolab PGSTAT 30 (Switzerland) instrument equipped with Frequency Response Analysis (FRA) software version 4.9. A deposition of approximately 6 µL of 1mM maleic anhydride onto the modified SPCE occurred for a brief period. Subsequently, the modified SPCEs were immersed in a solution containing 1 mM of $K_3Fe(CN)_6$ within 0.1 M KCl. Rapid EIS measurements were conducted on the modified SPCE/maleic anhydride configuration, requiring only about four minutes for completion [1,5, 9]. In contrast, CV typically involves a much shorter time frame of a few seconds.

The estimation of surface areas for modified SPCEs with maleic anhydride involved a comparison of fractional surface coverage (θ_{IS}^{p}), active site radius (r_a), and the distance between two adjacent sites ($2r_b$) values. Equations for impedance analysis in electrode studies have been developed by Matsuda et al. [17] and Finklea et al. [18], considering scenarios where θ values are either lower or higher than 0.9. These equations assumed equal concentrations and diffusion coefficients for the oxidized and reduced redox species. Finklea et al. [18] indicated that the equations for real Faradaic impedance exhibit similarity in both situations, differing primarily in the parameter q, which defines the correlation between the diffusion coefficient and microelectrode dimensions. For values of $(1 - \theta_{IS}^{p})$ greater than 0.1 and $(1 - \theta_{IS}^{p})$ less than 0.1, Equations (1), (2), and (3) describing the real Faradaic impedance are provided as follows:

$$Z'_f = \frac{R_{CT}}{1-\theta_{IS}^{p}} + \frac{\sigma}{\sqrt{\omega}} + \frac{\sigma}{1-\theta_{IS}^{p}}\left\{\frac{\left[(\omega^2+q^2)^{\frac{1}{2}}+q\right]}{(\omega^2+q^2)}\right\}^{\frac{1}{2}} \quad (1)$$

where σ, R_{CT}, and ω, and q can be attained from Eq. (2) – (4) [1, 5]:

$$\sigma = \frac{\sqrt{2RT}}{n^2F^2CA\sqrt{D}} \quad (2)$$

$$q = \frac{2D}{[r_b^2\theta_{IS}^{p}(1-\theta_{IS}^{p})\ln(1+\frac{0.27}{1-\theta_{IS}^{p}})^{\frac{1}{2}}]} \text{ for } (1-\theta_{IS}^{p}) > 0.1 \quad (3)$$

$$q = \frac{D}{0.36r_a^2} \text{ for } (1-\theta_{IS}^{p}) < 0.1 \quad (4)$$

The Faradaic impedance corresponding to high frequencies is defined by Eq. (5) [1, 5]:

$$Z'_f = \frac{R_{CT}}{1-\theta_{IS}^{p}} + m\omega^{-\frac{1}{2}} \quad (5)$$

where

$$m = \sigma + \frac{\sigma}{1-\theta_{IS}^{p}} \quad (6)$$

$$(1-\theta_{IS}^{p}) = \frac{ra^2}{rb^2} \quad (7)$$

 Surface Characterization of Modified SPCE/Maleic ydride

FESEM (Hitachi SU8020, Japan) was employed to demonstrate the attachment, size, and morphology of AuNPs–cysteine on the modified SPCE at a voltage of 10 kV. The haptenation for modified SPCEs/maleic anhydride was also studied using AFM (JPK BioAFM, Germany). The modified SPCE was analyzed on flat

surfaces evaporated onto silicon substrates through AFM imaging. Characterization of the modified SPCE also involved FTIR–ATR (Frontier PerkinElmer: Santa Clara, USA) analysis to detect the presence of AuNPs and cysteine from 650 to 4000 cm^{-1}.

Performance Analysis via Stability and Reproducibility Studies of Modified SPCE/Maleic Anhydride

To investigate their storage stability, the fabricated modified SPCEs were stored at 4 °C (refrigerator) and at room temperature for four weeks, without the use of any preservatives. To minimize air moisture, aluminium foil containing silica gel was employed. Throughout these experiments, each modified SPCE was individually stored in an aluminium foil package, and freshly prepared modified SPCEs were utilized for each EIS measurement session. Within this study, the R_{CT} readings could be regarded as a quantitative metric for evaluating repeatability. Repeatability investigations were conducted under optimal conditions by assessing R_{CT} with a consistent maleic anhydride concentration (40 mM), utilizing ten independently prepared ETSC modified SPCEs [1, 5, 9].

RESULTS AND DISCUSSION

Electrochemical Measurement of Maleic Anhydride with Modified SPCE

The modified SPCE and its interactions with maleic anhydride were analyzed using EIS and CV. EIS analyses were conducted for EC, ETSC, and ETSTSC modified SPCEs, and charge transfer resistance (R_{CT}) was measured. EIS is a technique sensitive to alterations on the surface of the modified electrode, making it useful for detecting interactions between maleic anhydride and cysteine on the modified SPCE. The binding event between maleic anhydride and cysteine changed the thickness of the cysteine layer, leading to an increase in R_{CT}. In this study, the SPCE was modified with multiple layers of AuNPs and cysteine to improve detection of maleic anhydride and produce a stable insulation layer on the modified SPCE. The EC, ETSC, and ETSTSC modified SPCEs were analyzed using an electric equivalent circuit R_S [R_{CT} (CPEW)]. This circuit consisted of solution resistance (R_S) connected in series with R_{CT} and parallel with a Warburg element (W) (diffusion resistance) and a constant phase element (CPE). The W element was not utilized in the EC, ETSC, and ETSTSC modified SPCEs with and without maleic anhydride due to the lack of the 45° line on the impedance spectra [12].

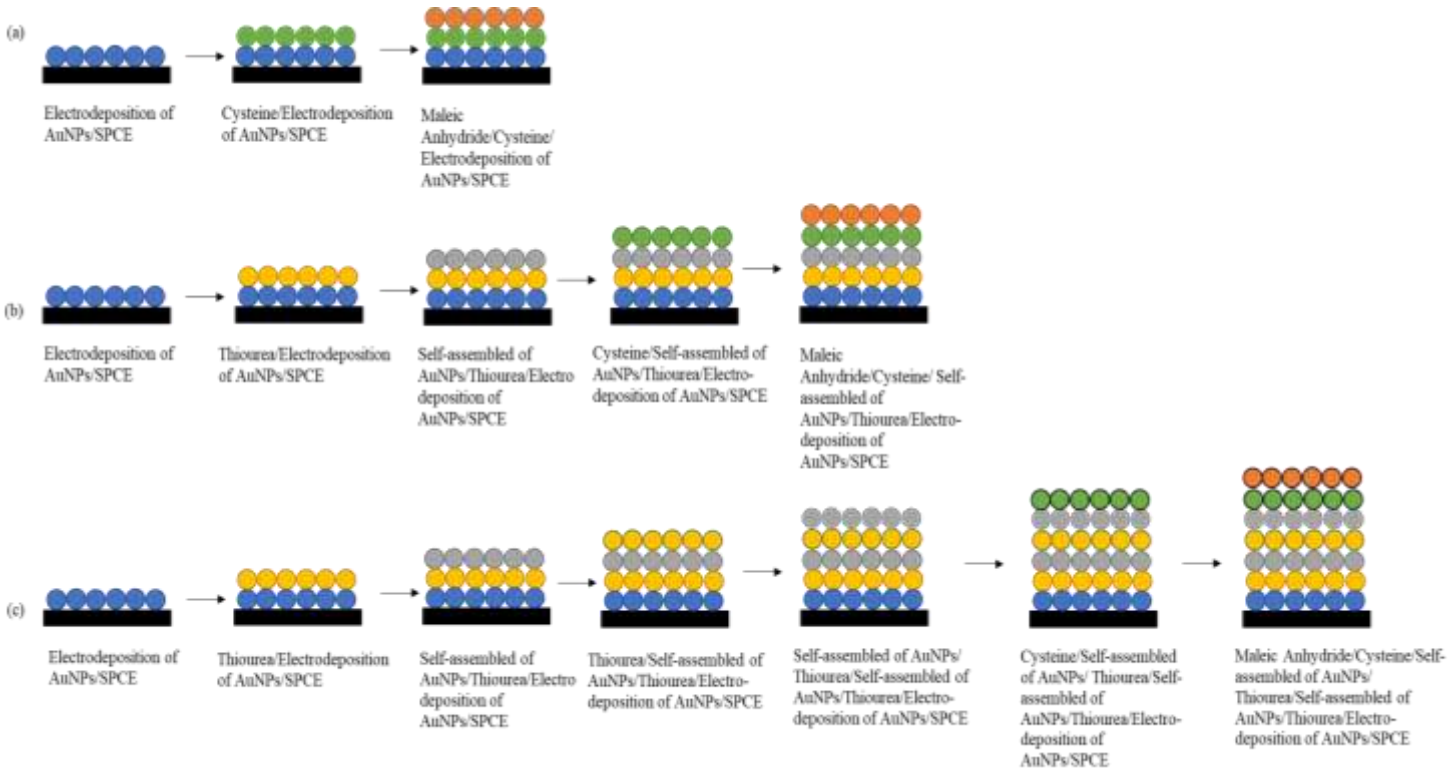

Figure 1. Illustration of (a) EC, (b) ETSC, and (c) ETSTSC modified SPCE. The compound notation is as follows: AuNPs (blue), thiourea (yellow), AuNPs (grey), cysteine (green), and maleic anhydride (orange) [1, 5].

As mentioned earlier, EC, ETSC, and ETSTSC modified SPCEs were analyzed to confirm the presence of multiple layers of AuNPs and cysteine embedded in the modified SPCEs (Figure 1). The Nyquist plots of EC, ETSC, and ETSTSC modified SPCEs (Figure 2) showed that the diameter of the semicircle increased with an increase in the monolayers. This indicated a significant barrier effect for the electron transfer reaction of $Fe(CN)_6^{3-/4-}$ when cysteine blocked the AuNP modified SPCE surface. The presence of multiple layers of AuNPs, thiourea, and cysteine on the modified SPCE indicated significant partial surface blocking and thicker layers [1, 5].

Significant changes in R_{CT} were observed based on the acquired comparative spectra for EC, ETSC, and ETSTSC modified SPCEs/maleic anhydride. The charge transfer of maleic anhydride ($R_{CT}^{maleic\ anhydride}$) in EC modified SPCE/maleic anhydride (31160.99 Ω) was lower than in EC modified SPCE (31493.50 Ω). Immobilization of EC modified SPCE/maleic anhydride caused a decrease in the charge transfer of $Fe(CN)_6^{3-/4-}$, resulting in a significant increase in $R_{CT}^{maleic\ anhydride}$; however, the electrochemical results of the EC modified SPCE/maleic anhydride were not significantly influenced after immobilization with maleic anhydride. The $R_{CT}^{maleic\ anhydride}$ values of EC modified SPCE/maleic anhydride did not increase compared to R_{CT} values before the immobilization of maleic anhydride (Figure 2 (a)). This may be due to slow electron transfer, and impedance is controlled by interfacial electron transfer [1, 3, 5, 9].

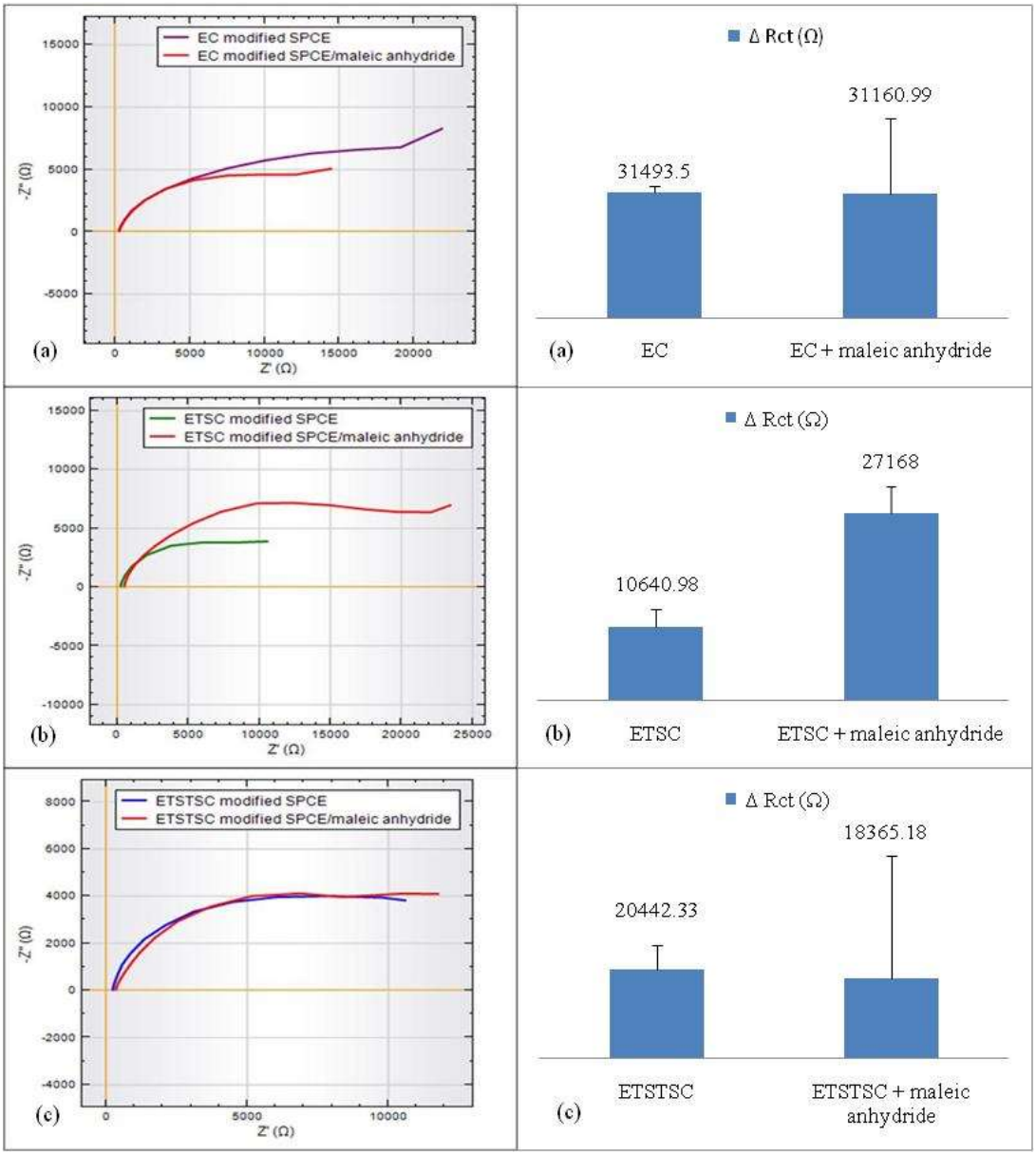

Figure 2. Nyquist plots and graphs of (a) EC, (b) ETSC, and (c) ETSTSC modified SPCE with/without maleic anhydride (n=3).

The $R_{CT}^{maleic\ anhydride}$ of ETSC modified SPCE/ maleic anhydride (27168.00 Ω) was greater when compared to ETSC modified SPCE. The increase in $R_{CT}^{maleic\ anhydride}$ may be a result of the effective attachment of maleic anhydride to the ETSC modified SPCE. The electron transfer between electrolyte redox active couple and the ETSC modified SPCE resulted in a higher $R_{CT}^{maleic\ anhydride}$ value. The saturation of the active $Fe(CN)_6^{3-/4-}$ redox species attached to cysteine resulted in a complex haptenation layer on the ETSC modified SPCE surface. It was postulated that the ETSC modified SPCE provided a full surface coverage area for maleic anhydride to attach to, leading to increased R_{CT}readings [9] (Figure 2 (b)).

The $R_{CT}^{maleic\ anhydride}$ of ETSTSC modified SPCE/maleic anhydride (18365.18 Ω) was lower compared to ETSTSC modified SPCE (20442.33 Ω) (Figure 2(c)). In this case, the $R_{CT}^{maleic\ anhydride}$ value did not increase after immobilization of ETSTSC modified SPCE/ maleic anhydride, probably because maleic anhydride did not act as a blocking layer to the cysteine due to the low surface coverage area that did not impede the electrode enough [1, 5]. The reduction in resistance exhibited a direct correlation with the thickness of the deposited material. Consequently, at a specific potential or voltage, the decrease in R_{CT} was proportional to the reduction in thickness [10].

The outcomes of the CV investigations are illustrated in Figure 3, highlighting the modifiable behaviour of the $Fe(CN)_6^{-3/-4}$ redox species by the modified SPCE. The cathodic peak current (I_{pc}) corresponded to the reduction process of the $Fe(CN)_6^{-3/-4}$ redox species. Assuming the redox process is fully reversible for the $Fe(CN)_6^{-3/-4}$ redox species (characterized by rapid electron transfer without kinetic limitations), the CV peak is broadly governed by the Nernst equation once the point of reversibility is reached. The peak materializes when the rate of the $Fe(CN)_6^{-3/-4}$ redox species supplied by the diffusion gradient becomes insufficient, leading to a decline in current [19]. As time progresses, the diffusion layer thickness increases, causing a reduction in the diffusion gradient. Consequently, the current progressively decreases from the peak, eventually entering a diffusion–limited region [7].

The results of CV studies are presented in Figure 3 based on the amendable action of the modified SPCE with the $Fe(CN)_6^{-3/-4}$ redox species. The peak cathodic current (I_{pc}) corresponds to the reduction of the $Fe(CN)_6^{-3/-4}$ redox species. In the event that the $Fe(CN)_6^{-3/-4}$ redox process operates with full reversibility (an electron transfer probe not restricted by electron transfer kinetics), the CV peak is approximately determined by the Nernst equation once the reversible potential is achieved [12]. This peak occurs when the diffusion gradient becomes incapable of supplying $Fe(CN)_6^{-3/-4}$ redox species at a certain rate, leading to a decrease in the current. The diffusion gradient decreases as the diffusion layer thickness increases over time. As a result, the current decreases, transitioning to a diffusion–limited region after reaching the peak [19].

Figure 3 represents typical CV plots of the modified SPCE before and after exposure with maleic anhydride: EC, ETSC, and ETSTSC. The $Fe(CN)_6^{-3/-4}$ redox species in EC modified SPCE (Figure 3(a)) gave a peak cathodic current value of 6.5485 µA. The sharp peak cathodic current with maleic anhydride ($I_{pc}^{maleic\ anhydride}$) of 6.5485 µA for the EC modified SPCE was found to decrease significantly after exposure of the electrode to maleic anhydride (5.8198 µA). A slight shift in the cathodic potential to a slightly less positive value was also observed but without any changes in the shape of the curve.

Modifying the ETSC modified SPCE/maleic anhydride (Figure 3 (b)) shifted cathodic potentials to less positive values, increasing its intensity. This indicated a greater blockage of electron transfer reactions for $Fe(CN)_6^{-3/-4}$ redox species on the surface after modification with maleic anhydride. The modified SPCE layers hindered the access of electroactive $Fe(CN)_6^{3-/4-}$ redox species, therefore increasing the redox I_{pc} values. The inhibition of electron transport between $Fe(CN)_6^{-3/-4}$ redox species in solution and the ETSC modified SPCE may be the primary reason for the statistically significant difference seen for a particular CV curve in this manner. Compared to EC modified SPCE, thiourea was used as a binding agent for ETSC modified SPCE [20]. Thiourea may have enhanced the strength between the layers of modified SPCE.

The I_{pc} value (7.8142 µA) for the ETSTSC modified SPCE (Figure 3(c)) indicated a major barrier to the charge transfer reaction involving the $Fe(CN)_6^{3-/4-}$ a redox species, as a result of partial surface restriction and increased layer thickness. However, the sharp $I_{pc}^{maleic\ anhydride}$ value of 7.8162 µA decreased slightly to 7.3939 µA after exposure to the ETSTSC modified SPCE/maleic anhydride. This might be because maleic anhydride was not fully immobilized on the ETSTSC modified SPCE, as the surface coverage was less stable when the $Fe(CN)_6^{-3/-4}$ reduction process occurred. Deposition of maleic anhydride on the surface of ETSTSC modified SPCE caused a conversion; however, the peak current was lowered. As a result, the CV curves would not give the appropriate expected changes in ETSTSC modified SPCE/maleic anhydride.

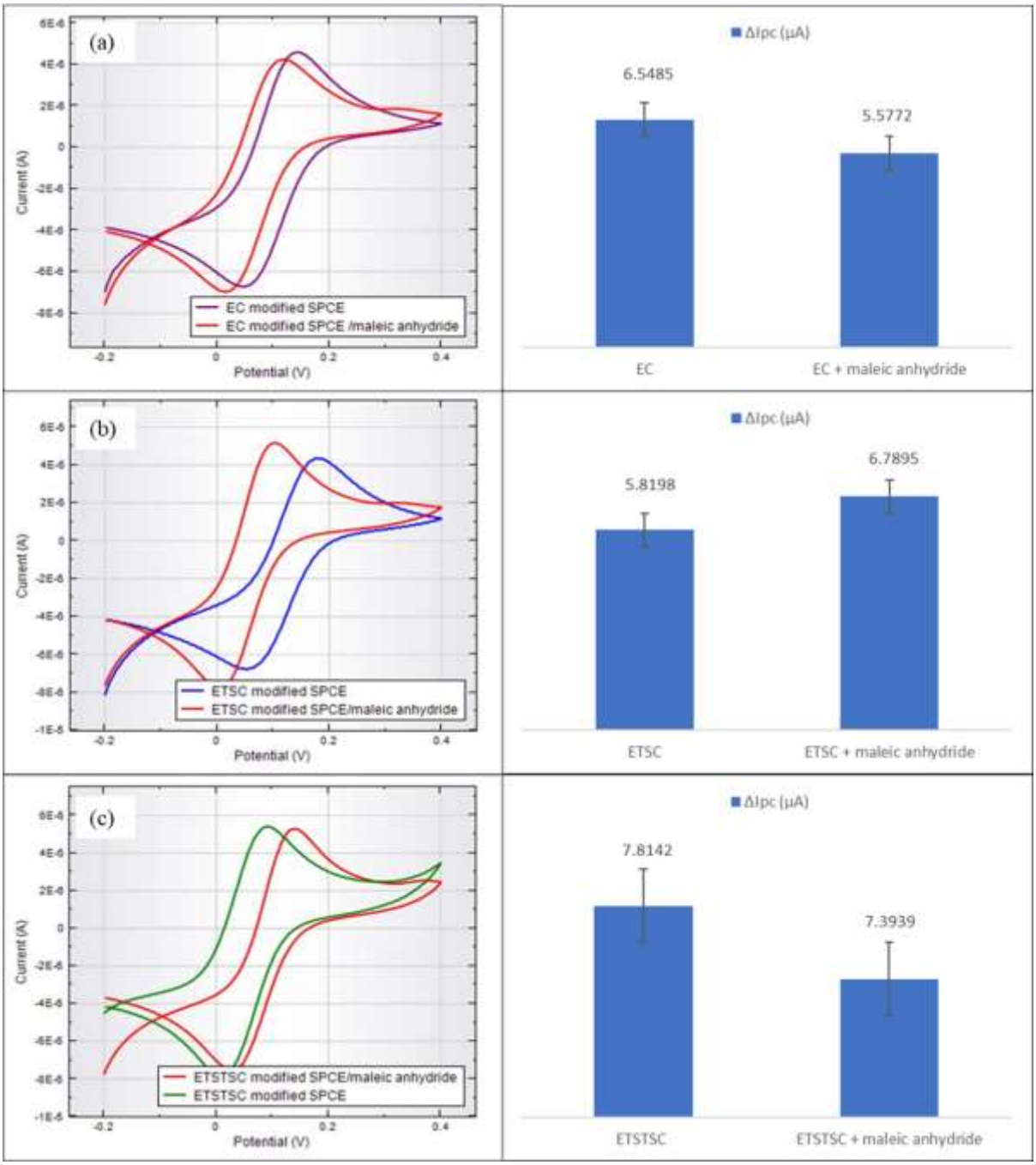

Figure 3. Typical CV plots for modified SPCE: (a) EC, (b) ETSC, and (c) ETSTSC with and without maleic anhydride

The addition of cysteine, thiourea, and AuNPs resulted in higher I_{pc} values for ETSC modified SPCE. The self–assembly and electrodeposition method for AuNPs on thiourea and cysteine showed better results compared to EC and ETSTSC modified SPCE. This may be explained by the increase in electron transfer between the $Fe(CN)_6^{3-/4-}$ redox species, resulting in a higher value of I_{pc} for the insulating layer on the ETSC modified SPCE. Additionally, the high stability between the combination of the immobilization layers of cysteine, thiourea, and AuNPs on ETSC modified SPCE contributed to the results of I_{pc}. This is in agreement with the findings reported by Noh and Abd Aziz [21].

The $Fe(CN)_6^{-3/-4}$ redox species is extensively used in CV for kinetics studies on the characterization of electrode surfaces [6]. Aside from ensuring that the cysteine and AuNPs preserve their functionality, the immobilization process must also ensure that the active site is easily accessible. For effective electron transfer, it is also necessary that the cysteine and the transducer be in close contact with one another [13].

However, these measures are unstable and cannot be recognized as a diagnostic approach for confirming skin sensitization analysis. Using CV, SAMs obtained for modified SPCE may be more appropriately described by comparing the magnitude of current or anodic peak intensities in a solution containing an electroactive redox species ($Fe(CN)_6^{-3/-4}$).

In this work, ETSC modified SPCE showed the highest I_{pc} (from the CV) and R_{CT} (from EIS) readings compared to EC and ETSTSC modified SPCE, indicating the existence of a stable insulation layer when the maleic anhydride came in contact with the surface of the modified electrode. Consequently, the collected data established the suitability of the ETSC modified SPCE for further exploration within this study. Furthermore, EIS measurements were identified as more appropriate for the detection of maleic anhydride for skin sensitization assessment. In the skin sensitization process, protein haptenation occurs through the formation of stable adducts between hapten (maleic anhydride) and endogenous peptides (cysteine) within the skin. This theoretical foundation underscores the potential of any sensitizer capable of forming enduring hapten–peptide conjugates to induce skin sensitization. The $\Delta R_{CT}^{maleic\ anhydride}$ elucidates the degree of electrostatic interaction between $Fe(CN)_6^{3-/4-}$ and maleic anhydride, revealing insights into the modified SPCE's electron transfer capability for the haptenation process.

Estimation of θ_{IS}^{p}, r_a, and the $2r_b$ on Modified SPCE/Maleic Anhydride

The estimated values for θ_{IS}^{p}, r_a, and $2r_b$ were derived under the assumption that charge transfer transpired at r_a and that planar diffusions of $Fe(CN)_6^{-3/-4}$ existed towards these sites, in accordance with the model presented in Figure 4(a). This study aimed to determine the optimal R_{CT} for achieving high surface coverage on the modified SPCE, maximizing its capability to detect maleic anhydride. The proposed equivalent circuit (R(Q[R(QR)])) was similarly fitted to the impedance experimental data for EC, ETSC, and ETSTSC modified SPCEs with maleic anhydride. However, it is noteworthy that the mass transfer impedance did not precisely manifest as a true Warburg impedance, as illustrated in Figure 4(b). Table 1 provides insight into the EC, ETSC, and ETSTSC modified SPCEs with maleic anhydride, revealing that α_1 exceeded the threshold of 0.9. The semicircle diameters reflected the charge transfer reaction observed at higher frequencies, which was succeeded in the (–Z") vs. (Z') plot by a linear region at lower frequencies. Within this frequency range, the impedance response was predominantly influenced by the mass transfer of $Fe(CN)_6^{-3/-4}$ to and from the modified SPCE surface [7].

Within this circuit arrangement, R_S represents the solution resistance, and R_{CT} signifies the charge transfer resistance associated with the oxidation and reduction mechanisms of the $Fe(CN)_6^{3-/4-}$ redox species. CPE1 denotes either the capacitance of the double layer or the combined capacitance within the sequence of the coated electrode/solution interface. W, denoted by CPE2 and diffusion resistance (R_D), is encompassed within this characterization. The standard capacitor was substituted with CPE1 owing to the non–uniform current distribution over the SPCE surface. This unevenness arises from the surface's roughness, defects, and non–homogeneities. The incorporation of a CPE with α>0.5, connected in parallel with R_D, effectively characterizes the diffusion impedance and accounts for the finite length of the diffusion path. The sub–circuit (R_D CPE2) is directly tied to mass transport dynamics, perturbed by the presence of the cysteine–AuNP layer on the modified SPCE [1, 21].

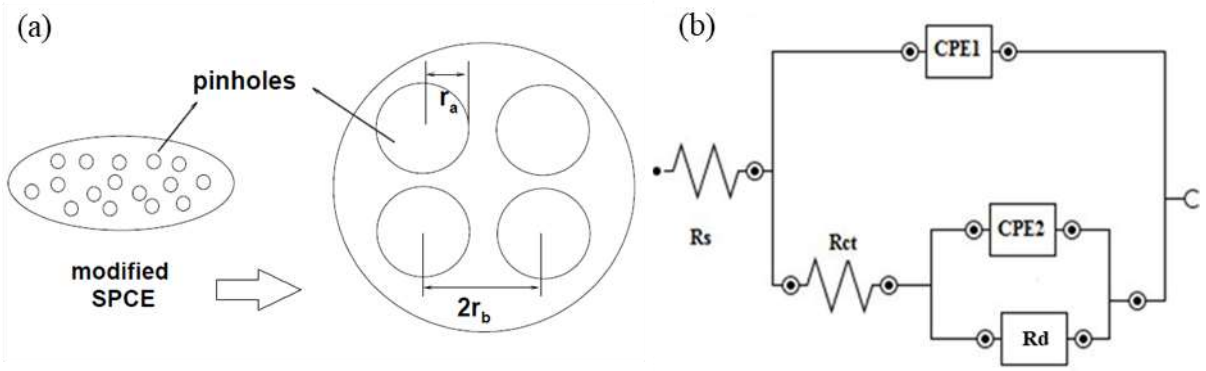

Figure 4. (a) Schematic representation of a pinhole/defect arrangement model with r_a and $2r_b$ surrounding the microarray electrode. (b) Equivalent ideal Randles circuit that was modified.

Table 1. Impedance parameters used with modified SPCE/maleic anhydride.

Type of modified SPCE	Rs (Ωcm^2)	CPE1 ($\mu Scm^2 \cdot S^{\alpha-1}$)	α_1	$R_{CT.app}$ (Ωcm^2)	CPE2 ($\mu Scm^2 \cdot S^{\alpha-1}$)	α_2	R_d (Ωcm^2)
EC + maleic anhydride	28.09	3.60	0.78	1339.65	29.54	0.66	1455.33
ETSC + maleic anhydride	22.39	1.44	0.92	4097.83	11.09	0.40	773.34
ETSTSC + maleic anhydride	16.64	3.31	0.27	24.65	7.76	0.81	2063.98

$$R_{CT.app} = \frac{R_{CT}}{(1-\theta)}, \text{ capacitance} = CPE\ (\omega_{max})^{\alpha-1}$$

Evaluation of the charge transfer process occurring at the modified SPCE may be used to determine the stability of the modified SPCE, which is a critical component in the creation of electrochemical sensors. Thiol (from cysteine) groups quickly adsorbed on the AuNP layer surfaces, forming covalent bonds over time. The AuNP layer was infrequently perfect even though it was highly oriented and densely packed. The AuNP layer coated on the modified SPCE resembled a microarray electrode. There were pinholes/defects in the fabrication of modified SPCE, resulting from imperfect adsorption of the thiol on the AuNP layer surface during the self–assembly step and/or subsequent loss during rinsing or storage. Molecules from the electrolyte ($Fe(CN)_6^{3-/4-}$ redox species) can reach the electrode surface across the pinholes/defects. The impedance readings showed information on the distribution of pinholes/defects and the surface coverage of haptenation with maleic anhydride [1, 5].

This study further explored the calculation of θ_{IS}^{p} for EC, ETSC, and ETSTSC modified SPCE with maleic anhydride, including the pinholes/defects. θ_{IS}^{p} was expected to be influenced by the surface roughness, r_a, and $2r_b$. When the r_a to microarray electrode occurred, the charge transfer reaction observed was not a simple function of the exposed area of the modified SPCE. The distribution and r_a size of the pinholes/defects adequately influenced the surface structure and its effects on electron transfer of maleic anhydride [1, 5, 20–21].

By considering the following conditions, the estimated dimensions of pinholes/defects, θ_{IS}^{p}, and the diffusion coefficients of the $Fe(CN)_6^{-3/-4}$ redox species can be determined: (1) Ensuring $\alpha_1 \geq 0.9$ to permit the replacement of CPE1 with a capacitor; (2) Noting the linear behaviour of complex plane plots observed at the onset of the second capacitive loop, implying mass transport control in the low–frequency region; (3) Acknowledging that the EC, ETSC, and ETSTSC modified SPCEs exposed to maleic anhydride could be regarded as forming active sites with a radius r_a, where the oxidation and reduction electron transfer reactions of a redox species might occur. The pinholes/defects corresponded to the unmodified surface of the modified SPCE, encompassing a total area $A(1-\theta_{IS}^{p})$, where A represents the working surface area of the modified SPCE. The distances between adjacent active sites were $2r_b$, where r_b indicated the radius of the inactive domain encircling the pinhole; (4) The r_a was encircled by an inactive region (modified SPCE without pinholes/defects), leading to the total inactive area $A\theta_{IS}^{p}$; (5) The diffusion of $Fe(CN)_6^{-3/-4}$ redox species towards the regions of the modified SPCE was envisaged as planar, with diffusion treated as semi–infinite [1].

When $\omega = 0$, σ and R_{CT} can be approximated from the slope and intercept of the Faradaic impedance plot, (Z'_f) vs. $\omega^{-1/2}$, respectively (depicted in Figure 5) for the EC, ETSC, and ETSTSC modified SPCEs exposed to maleic anhydride. Utilizing Equation (2), a $Fe(CN)_6^{-3/-4}$ redox species diffusion coefficient, $D = 1.21\times10^{-8}\ cm^2 \cdot s^{-1}$ was obtained. Considering that a precise R_S correction can be readily applied, all the pertinent parameters can be deduced by analyzing the high and low frequency regions of the real Faradaic impedance plots, Z'_f vs. $\omega^{-1/2}$. For such an assessment, the q value can also be derived from the intersection of lines in the high and low frequency domains of (Z'_f) as = q/2, and the closest spacing between pinholes/defects can be estimated using Equation (3) or (4), as proposed by Matsuda et al. [17].

Using the same method, the θ_{IS}^{p} values for both ETSTSC and EC modified SPCE exposed with maleic anhydride were estimated to be 0.67 and 0.36, respectively. The intersection of the high and low frequency domains yielded q values of 240 and 340, respectively, for the EC modified SPCE (Figure 5(a)) and ETSTSC modified SPCE (Figure 5(c)). Thus, for ETSTSC modified SPCE, the values of r_a and $2r_b$ were 11.55 µm and 40.20 µm, respectively, while for EC modified SPCE, the values of r_a and $2r_b$ were 24.64. µm and 61.60 µm, respectively (Table 2).

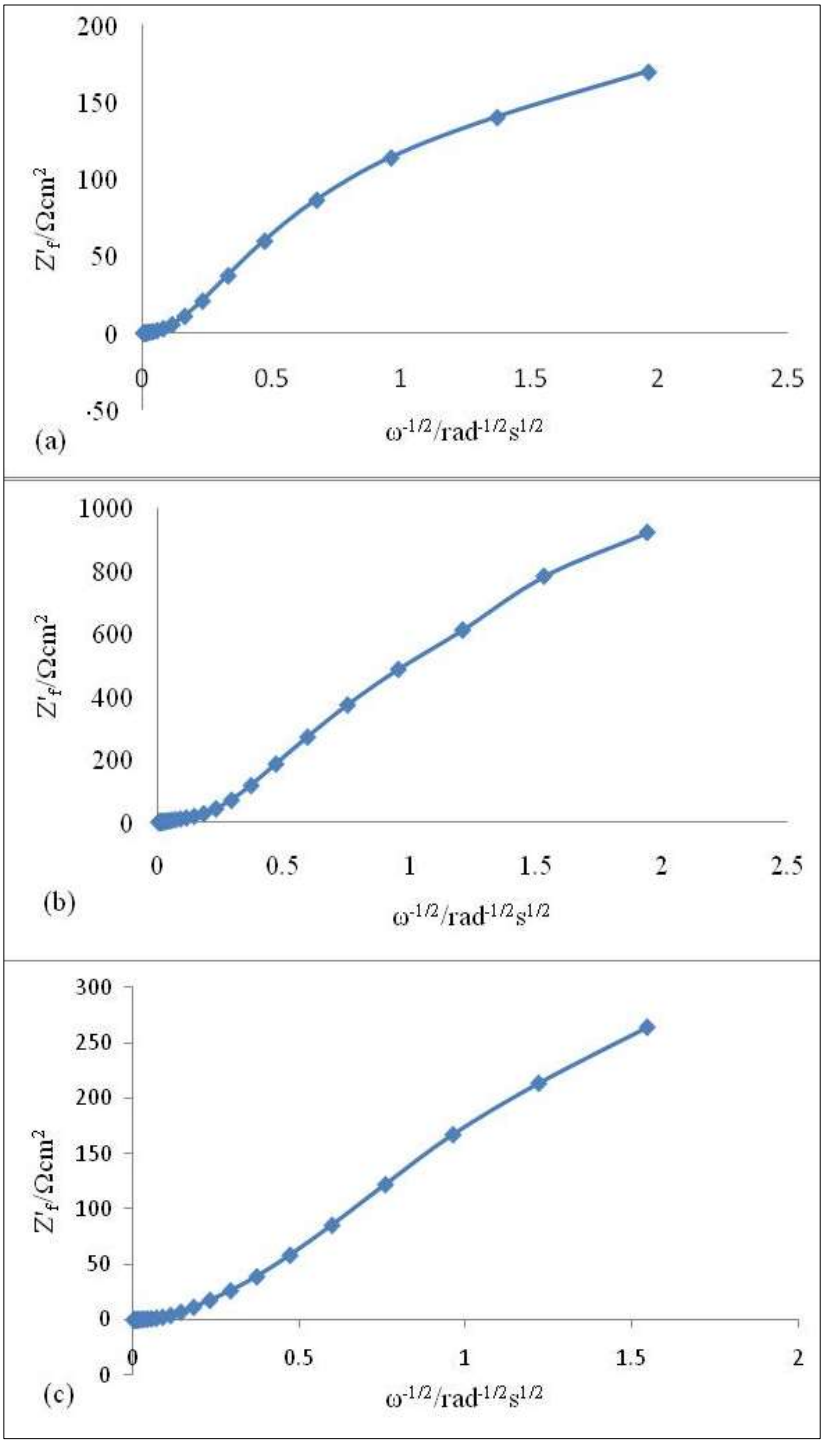

Figure 5. Faradaic impedance plots, Z'_f and $\omega^{-1/2}$: (a) EC, (b) ETSC and (c) ETSTSC modified SPCE with maleic anhydride.

Table 2. Comparison of θ_{IS}^{p}, r_a and $2r_b$ results that fit the experimental data.

Type of modified SPCE	θ_{IS}^{P}	Slope, m (Ωcm^2 $rad^{1/2}s^{-1/2}$)	r_a (µm)	$2r_b$ (µm)
EC+ maleic anhydride	0.36	496.61	24.64	61.60
ETSC+ maleic anhydride	0.98	1274.52	2.5	35.36
ETSTSC+ maleic anhydride	0.67	103.76	11.55	40.2

Figure 5(b) shows that for ETSC modified SPCE exposed with maleic anhydride, from the slope of the Z'_f vs. $\omega^{-1/2}$ plot in the high frequency region with $\theta_{IS}^{p} = 0.98$ was found, and a value of m = 1274.52 $\Omega cm^2 \cdot rad^{1/2} \cdot s^{-1/2}$ was obtained. The value q = 5400 was determined via the intersection of the high and low frequency domains. Using Equation (3), the radius r_a and $2r_b$ were calculated as 2.5 µm and 35.36 µm (Equation 7). As seen in Table 2, after the EC, ETSC, and ETSTSC modified SPCE were exposed to maleic anhydride, the θ_{IS}^{p}, r_a and $2r_b$ values changed. θ_{IS}^{p} of EC and ETSTSC modified SPCE decreased after being exposed to maleic anhydride.

At the same time, the SAM probably became thin and the pinhole/defect sizes (r_a and $2r_b$) increased after EC and ETSTSC modified SPCE were exposed to maleic anhydride. This may be due to the haptenation of maleic anhydride on the EC and ETSTSC modified SPCE that did not show satisfactory results (i.e., an increase of R_{CT} readings (Table 2)). Thus, the EC and ETSTSC modified SPCE seemed to be unsuitable for the haptenation detection experiments. The increase in θ_{IS}^{p} also corresponded to the increase in R_{CT} readings for ETSC modified SPCE/maleic anhydride (Table 2). It was deduced that a charge transfer reaction between maleic anhydride and cysteine had occurred since a response corresponding to a haptenation process was observed. A possible explanation for such an occurrence could be that the SAMs became densely packed (highly oriented), and the pinhole/defect size decreased after ETSC modified SPCE was exposed to maleic anhydride. The ETSC modified SPCE was postulated to exhibit higher stability in terms of SAM after haptenation with maleic anhydride compared to EC and ETSTSC modified SPCE [1, 21].

These values were deemed estimations, rooted in the initial assumptions made before the calculations were conducted. After considering the impedance data of modified SPCE exposed with maleic anhydride, ETSC modified SPCE was estimated to have fewer pinholes/defects and higher surface coverage compared to EC and ETSTSC modified SPCE. Hence, the ETSC modified SPCE was a suitably modified layer for subsequent experiments.

The Effect of Maleic Anhydride Concentration on Haptenation for Modified SPCE

In skin sensitization applications, a suitable and precise detection method is imperative. Analysis of the EIS data highlighted the pronounced elevation in R_{CT} values for the ETSC modified SPCE following interaction with maleic anhydride, in contrast with EC and ETSTSC modified SPCE. This substantial increase underscored the establishment of a robust insulation layer upon the electrode's engagement with maleic anhydride. Consequently, the ETSC modified SPCE emerged as the optimal candidate for further exploration within this study. Delving into Figure 6, it became evident that the $\Delta R_{CT}^{maleic\ anhydride}$ metric exhibited negligible fluctuations across diverse concentrations of ETSC modified SPCE/maleic anhydride. This observation implied that varying maleic anhydride concentrations exerted minimal influence on $\Delta R_{CT}^{maleic\ anhydride}$ values within the ETSC modified SPCE/maleic anhydride context. This phenomenon was ascribed to the established role of cysteine reactivity, which was pivotal in the evolution of the ETSC modified SPCE for skin sensitization assessment. Notably, the electrophilic properties of maleic anhydride enabled its interaction with a spectrum of nucleophiles, fostering the formation of covalent bonds [1, 5].

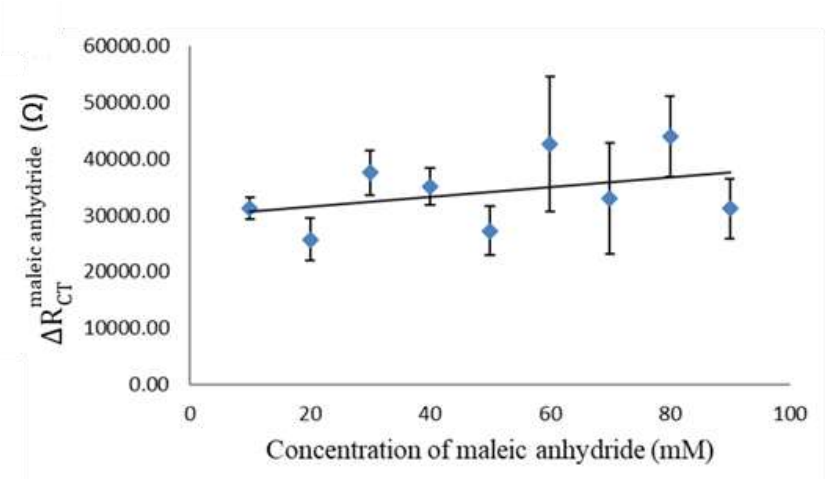

Figure 6. Concentration of ETSC modified SPCE/maleic anhydride vs. $\Delta R_{CT}^{maleic\ anhydride}$.

In this study, an ETSC modified SPCE was developed to detect maleic anhydride. While the sensor could not detect changes in maleic anhydride concentration, it consistently provided the expected optimum value but was unable to provide limits of detection. This observation prompted the consideration of several possibilities. One explanation is that the ETSC modified SPCE may have reached its maximum detection capacity or saturation point for maleic anhydride. This implied that the sensor exhibited a robust response within a defined concentration range (10 to 90 mM), beyond which further differentiation was not feasible. Alternatively, the ETSC modified SPCE might have been operating optimally within its designated range, showcasing peak accuracy and consistency. As a result, any concentration variations within this range might have remained undetected due to the sensor already functioning at its highest level of performance. Moreover, it was conceivable that the ETSC modified SPCE was configured to detect concentrations surpassing a predetermined threshold value. Below this threshold, any alterations in concentration may not have triggered a noticeable response, resulting in a consistent, anticipated value being provided by the sensor. While the ETSC modified SPCE's ability to deliver the expected optimum value consistently suggested that it was fulfilling its intended function, its inherent limitation in detecting changes in concentration could potentially limit its applicability in scenarios where sensitivity to subtle variations is essential. This limitation is particularly noteworthy since the ETSC modified SPCE was specifically designed to detect maleic anhydride, which is reactive to cysteine haptenation [1, 5].

The sensitivity demonstrated by the ETSC modified SPCE/maleic anhydride combination became apparent through its consistent response across maleic anhydride concentrations, indicating a moderate sensitivity level. Remarkably, this concentration range evoked minimal impact on $\Delta R_{CT}^{maleic\ anhydride}$ readings. However, the absence of a discernible slope precluded the calculation of a detection limit for the ETSC modified SPCE/maleic anhydride [22]. Notably, the trend lines connecting data points from varying concentrations of maleic anhydride exhibited an almost horizontal alignment, culminating in an exceedingly shallow slope [23]. This observation was particularly relevant given that the value was expected to fall within that range due to the nature of the maleic anhydride being monitored. Maleic anhydride, belonging to the extreme/high skin sensitizer class, typically triggers allergic reactions at concentrations known to be significant. As such, the sensor's moderate sensitivity was appropriate for applications where capturing moderate changes or variations was sufficient, and the detection of trace amounts or minor fluctuations was not a primary requirement.

Surface Characterization of Modified SPCE

From the FESEM image in Figure 7(a), it was evident that the formation of AuNPs–cysteine on the modified SPCE surface could be proved, as cysteine appeared to immobilize with AuNPs. The FESEM images also indicated that the ETSC modified SPCE exhibited a smooth surface with a non–uniform dispersion of AuNPs and cysteine molecules immobilized onto the carbon electrode surface [24]. A significant portion of the remaining cysteine molecules' attachment was ascribed to the covalent bonding between cysteine and the AuNPs. This interaction enhanced the probability of maleic anhydride attachment, with a robust interaction between Au–S on the carbon surface [8].

The haptenation of ETSC modified SPCE/ maleic anhydride was subjected to AFM investigation to determine surface images and morphology (Figure 7(b)). As a result of particle interactions, the AFM image showed a randomly packed structure. The results produced low spikes and peak spacing, showing that the surface had been topped with a thick layer and haptenation had occurred on ETSC modified SPCE/maleic anhydride. The peaks identified in Figure 7(c) corresponded to characteristic anhydride groups, with C=O bonds at 1474.39 and 1526.27 cm^{-1} and C−O bonds at 927.48 and 1058.05 cm^{-1}. These peaks strongly indicated the immobilization of maleic anhydride onto the surface of the ETSC modified SPCE. Additionally, the presence of C−S bond stretches at approximately 720.08 cm^{-1} and 680.08 cm^{-1} (Figure 7(d)) further suggested immobilization of cysteine on the surface of the ETSC modified SPCE [1].

The adsorption of ETSC modified SPCE/ maleic anhydride on the surface was speculated to be attributable to hydrogen bonding between the –SH functional groups and maleic anhydride's alkoxy and –SH functional groups. Maleic anhydride was exposed to ETSC modified SPCE as a strong/extreme potency skin sensitizer for skin sensitizing studies. The possible bond that may be formed from the binding of cysteine (through the sulphur bond) and maleic anhydride was hypothesized as a strong covalent bond through Michael acceptors (Figure 7(d)). Maleic anhydride was hypothesized to act as a Michael acceptor due to the presence of alkoxy groups [5] (Figure 7(e)). Further studies of cysteine and maleic anhydride mechanisms in skin sensitization studies might be compatible with *in silico* methods research using appropriate molecular docking data.

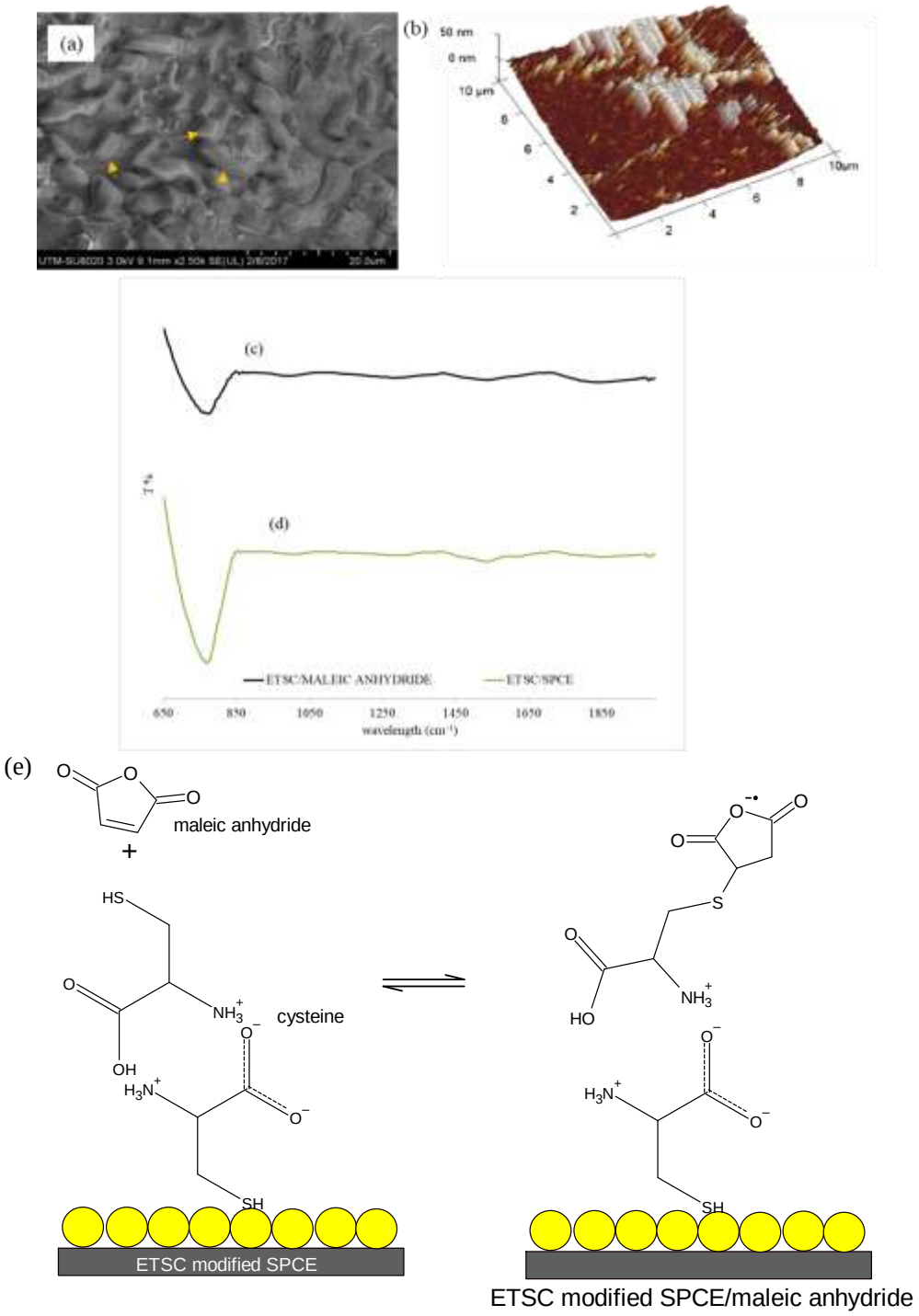

Figure 7. (a) FESEM image of ETSC modified SPCE (magnification of 2.50 k) (arrows indicate the immobilized cysteine), (b) 3D image of AFM of ETSC modified SPCE/maleic anhydride, (c, d) FTIR spectra of ETSC modified SPCE and ETSC modified SPCE/maleic anhydride, and (e) Possible binding mechanisms of ETSC modified SPCE/maleic anhydride.

Performance Analysis via Stability and Reproducibility Studies of Modified SPCE/Maleic Anhydride

In the context of storage stability assessment, the R_{CT} readings demonstrated a gradual decrease throughout the study period. The R_{CT} response of the sensor exhibited only a minor reduction of 10 % from its initial signal after being stored for 7 days in a dry state, both at room temperature and in a refrigerator, for the ETSC modified SPCE. When considering storage temperature, decomposition occurred at a slower rate at room temperature compared to 4 °C. Interestingly, a notable alteration in the initial signal, exceeding 10

%, was observed after the initial week, indicating a significant level of decomposition during extended storage of the ETSC modified SPCE in aluminium foil packaging. This decomposition could affect the sensor's functionality and reliability, potentially limiting the effectiveness of the redox–based detection methods that rely on the stability of the sensor's components. Notably, the efficacy of redox–based detection methods might also be constrained due to the potentially destabilizing impact of redox agents on the stability of cysteine and AuNPs on the surface of the modified SPCE, particularly after a storage period of four weeks [25].

Ensuring repeatability held the utmost significance, as it directly influenced the detection limit for the modified SPCE in sensitizer detection. The relative standard deviation (RSD) for the repeatability of ETSC modified SPCE with maleic anhydride was determined to be 9.49 %. The measurements of $R_{CT}^{maleic\ anhydride}$ underscored that the binding of maleic anhydride to cysteine (within the ETSC modified SPCE) could be effectively discerned in the presence of redox agents, particularly within specific frequency ranges [9]. By employing meticulously defined covalent chemistry to establish a connection between maleic anhydride and cysteine surfaces, the ETSC modified SPCE demonstrated the capacity to generate exceedingly reproducible surfaces conducive to accurate detection.

CONCLUSION

Our findings demonstrated the effective complexation of ETSC modified SPCE/maleic anhydride using EIS due to the significant R_{CT} response as the haptenation process occurred. Results from the CV and EIS methods indicated that the modified SPCE developed by EC and ETSTSC was insufficient for this purpose. The experimental results supported the hypothesized strong covalent bond mechanism between maleic anhydride and cysteine through Michael acceptors. The morphological alterations observed in the FESEM, AFM and FTIR–ATR measurements indicated the immobilization of maleic anhydride and cysteine through haptenation. The ETSC modified SPCE demonstrated improved stability and a slower decomposition rate when stored at room temperature compared to cold storage (4 °C) in the short term (up to 7 days). The ETSC modified SPCE/maleic anhydride also showed good reproducibility with a deviation of less than 10 %. Our work suggests the potential use of this detection test kit in future prototype applications for skin sensitization investigations. Further *in silico* studies of maleic anhydride with cysteine may be warranted to understand the mechanism better. The modified SPCE is positioned to advance the detection of over 100 diverse chemicals contributing to skin sensitization in the future.

ACKNOWLEDGEMENTS

This work was supported by Universiti Teknologi Malaysia through the FRGS grant (Vot: Q.J130000. 2546.14H71) and the Ministry of Higher Education (MyBrain scholarship).

REFERENCES

1. Noh, T. U., Abd. Aziz, A. (2022) Haptenation of skin sensitizers with cysteine and gold nanoparticles modified screen printed carbon electrode analyzed using impedance technique. *Journal of Electroanalytical Chemistry*, **907**, 116035.

2. Corea, N., Corvaro, M., Kluxen, F. M., Grivel, A., Morgan, N., Wiemann, C., Basketter, D. (2023) Assessing the risk of induction of skin sensitisation to plant protection products: A quantitative approach. *Regulatory Toxicology and Pharmacology*, **141**, 105408.

3. Noh, T. U., Abd. Aziz, A. (2021) The possibility of employing cysteine and gold nanoparticles for skin sensitization analysis: current status. *Journal of Research in Nanoscience and Nanotechnology*, **4(1)**, 1–12.

4. Pemberton, M. A., Kimber, I. (2023) Propylene glycol, skin sensitisation and allergic contact dermatitis: A scientific and regulatory conundrum. *Regulatory Toxicology and Pharmacology*, **138**, 105341.

5. Noh, T. U., Abd. Aziz, A. (2022) The correlation of haptenation of gold nanoparticles and cysteine modified screen printed carbon electrode by impedance technique with local lymph node assay data. *Toxicology in vitro*, **84**, 105433.

6. Orazem, M. E., Tribollet, B. (2020) A Tutorial on Electrochemical Impedance Spectroscopy. *ChemTexts*, **6(2)**, 12.

7. Barsoukov, E., MacDonald, J. R. (2018) *Impedance Spectroscopy: Theory, Experiment, and Applications, 2nd ed.; Wiley–VCH*.

8. Vu, Q. K., Tran, Q. H., Vu, N. P., Anh, T. L., Le Dang, T. T., Matteo, T., Nguyen, T. H. H. (2021) A label–free electrochemical biosensor based on screen–printed electrodes modified with gold nanoparticles for quick detection of bacterial pathogens. *Materials Today Communications*, **26**, 101726.

9. Noh, T. U., Abd. Aziz, A., Mahmad, A., Badrol, N. (2022) Impedance–based haptenation of skin sensitizers with a self–assembled monolayer of gold nanoparticles and cysteine modified screen

printed carbon electrode. *Inorganic Chemistry Communication*, **145**, 109964.

10. Amouzadeh Tabrizi, M., Acedo, P. (2022) An Electrochemical impedance spectroscopy–based aptasensor for the determination of SARS–CoV–2–RBD using a carbon nanofiber–gold nanocomposite modified screen–printed electrode. *Biosensors*, **12(3)**, 142.

11. Pajkossy, T. (2020) Voltammetry coupled with impedance spectroscopy. *Journal of Solid State Electrochemistry*, **24**, 2157–2159.

12. Edward, P. R. (2018) A cross examination of electron transfer rate constants for carbon screen–printed electrodes using electrochemical impedance spectroscopy and cyclic voltammetry. *Electrochimica Acta*, **286**, 179–186.

13. Gharbi, O., Tran, M. T. T., Tribollet, B., Turmine, M., Vivier, V. (2020) Revisiting cyclic voltammetry and electrochemical impedance spectroscopy analysis for capacitance measurements. *Electrochimica Acta*, **343**, 136109.

14. Wang, S., Zhang, J., Gharbi, O., Vivier, V., Gao, M., Orazem, M. E. (2021) Electrochemical Impedance Spectroscopy. *Nature Reviews Methods Primers*, **1**, 41.

15. Magar, H. S., Hassan, R. Y. A., Mulchandani, A. (2021) Electrochemical Impedance Spectroscopy (EIS): Principles, Construction, and Biosensing Applications. *Sensors*, **21**, 6578.

16. Nakayama, K., Zifle, A., Fritz, S., Fuchs, A., Sakaguchi, H., Miyazawa, M. (2023) Incorporating integrated testing strategy (ITSv1) defined approach into read–across (RAx) in predicting skin sensitisation potency: ITSv1–based RAx. *Regulatory Toxicology and Pharmacology*, **139**, 105358.

17. Matsuda, H., Tokuda, K., Gueshi, T. (1979) Voltammetry at partially covered electrodes: Part III. Faradaic impedance measurements at model electrodes. *Journal of Electroanalytical Chemistry*, **102**, 41–48.

18. Finklea, H. O., Sinder, D. A., Fedyk, J., Sabatini, E., Gaini, Y., Rubinstein, I. (1993) Characterization of octadecanethiol–coated gold electrodes as microarray electrodes by cyclic voltammetry and AC impedance spectroscopy. *Langmuir*, **9**.

19. Pajkossy, T., Mészáros, G. (2020) Connection of CVs and impedance spectra of reversible redox systems, as used for the validation of a dynamic electrochemical impedance spectrum measurement system. *Journal of Solid State Electrochemistry*, **24**, 2883–2889.

20. Noh, T. U., Abd. Aziz, A. (2017) Characterization of screen–printed carbon electrode modified with gold nanoparticles and cysteine. *In International Postgraduate Symposium in Biotechnology 2017*, 18–24.

21. Noh, T. U., Abd. Aziz, A. (2018) Estimation of the surface area of a screen–printed carbon electrode modified with gold nanoparticles and cysteine using electrochemical impedance spectroscopy. *Chemical Engineering Transactions*, **63**, 529–534.

22. Harahsheh, T., Makableh, Y. F., Rawashdeh, I., Al–Fandi, M. (2021) Enhanced aptasensor performance for targeted HER2 breast cancer detection by using screen–printed electrodes modified with Au nanoparticles. *Biomedical Microdevices*, **23(4)**, 1–11.

23. Shariati, M., Ghorbani, M., Sasanpour, P., Karimizefreh, A. (2018) An ultrasensitive label free human papilloma virus DNA biosensor using gold nanotubes based on nanoporous polycarbonate in electrical alignment. *Analytica Chimica Acta*, **1048**, 31–41.

24. Li, R., Li, Z., Wang, G., Gu, Z. (2018) Octadecylamine–functionalized graphene vesicles based voltammetric sensing of hydroquinone. *Sensors and Actuators B: Chemical*, **276**, 404–412.

25. Wang, W., Yi, Z., Liang, Q., Zhen, J., Wang, R., Li, M., Zeng, L., Li, Y. (2023) In situ deposition of gold nanoparticles and L–cysteine on screen–printed carbon electrode for rapid electrochemical determination of As(III) in water and tea. *Biosensors*, **13**, 130.